

## PARSEC-SCALE CIRCULAR POLARIZATION OBSERVATIONS OF 40 BLAZARS

DANIEL C. HOMAN<sup>1</sup>, JOANNE M. ATTRIDGE<sup>2</sup>, AND JOHN F. C. WARDLE<sup>1</sup>*Accepted for publication in ApJ*

## ABSTRACT

We present circular polarization results from a 5 GHz survey of the parsec-scale polarization properties of 40 AGN made with the VLBA. We find 11 circular polarization detections at the  $3\sigma$  level or higher. This nearly quadruples the number of sources detected in circular polarization at VLBI resolution. We find no correlation between fractional linear and circular polarization across our sample. A likely explanation is external Faraday depolarization in the cores of AGN which reduces linear polarization but leaves circular polarization unchanged. In comparing ours and other recent results to observations made  $\sim 20$  years ago, we find that, in five of six cases, sources have the same sign of circular polarization today as they did 20 years ago. This suggests the presence of a long term property of the jets, such as the polarity of a net magnetic flux, which is stable on time-scales much longer than those of individual outbursts.

*Subject headings:* galaxies: active – galaxies: jets – polarization

## 1. INTRODUCTION

Circular polarization (CP) observations of radio-loud active galactic nuclei (AGN) provide a unique opportunity, especially in conjunction with linear polarization observations, for constraining the magnetic field geometry, particle energy distribution, and even particle composition ( $e^+e^-$  vs.  $p^+p^-$ ) of their jets. A number of possible mechanisms have been proposed for the production of circular polarization in AGN (see Wardle & Homan (2001) and references therein). The two most likely are the *intrinsic* circular polarization of synchrotron radiation and Faraday *conversion* of linear to circular polarization, a propagation effect, e.g. Jones & O'Dell (1977). Weiler & de Pater (1983) catalog a large number of circular polarization observations of AGN, mainly from the 1970s, and find typical levels of  $\lesssim 0.1\%$ . After the survey by Komesaroff et al. (1984), there have been no major CP observations published until recently.

In Wardle et al. (1998), we reported the detection of circular polarization in the parsec-scale jet of 3C 279. Detailed analysis suggested the jet is predominately a pair plasma. Circular polarization has since been detected in the galactic center (Bower, Falcke & Backer 1999; Sault & Macquart 1999), the galactic X-ray binary SS433 (Fender et al. 2000), the intra-day variable source PKS 1519-273 (Macquart et al. 2000), and a sample of more than twenty AGN by Rayner, Norris & Sault (2000), hereafter RN&S. In Homan & Wardle (1999), hereafter H&W, we presented multi-epoch, parsec-scale CP detections of four AGN, made with the Very Long Baseline Array (VLBA)<sup>3</sup> at 15 GHz.

Here we present results from the first large scale circular polarization survey made at Very Long Baseline Interferometry (VLBI) resolution. In December 1996, we observed a sample of 40 AGN at 5 GHz ( $\lambda$  6 cm) with the VLBA. These observations were originally made as part of a continuing study of the parsec-scale linear polarization properties of blazars (Attridge (1999); Attridge et al., in prep.). They do not comprise a complete sample. We report the results of a re-analysis of these data

for circular polarization.

## 2. OBSERVATIONS AND CALIBRATION

The observations were scheduled in a continuous 48 hour block, with source changes after every 5.5 minute scan. Sources were highly interleaved in the schedule to maximize (u,v)-coverage. Each source was observed for at least ten scans, five on each day, giving a total integration time of nearly an hour<sup>4</sup>. The data were recorded at each station using 1-bit sampling and were correlated at the VLBA correlator in Socorro, NM. The correlated data contained all four cross-correlations (RR, RL, LR, LL), each with four intermediate frequencies (IFs). The data were loaded into NRAO's Astronomical Imaging Processing System (AIPS) (Bridle & Greisen 1994; Greisen 1988) and calibrated using standard techniques for VLBI polarization observations, e.g., (Cotton 1993; Roberts, Wardle & Brown 1994). The VLBA station in Hancock, NH was found to have a low flux calibration and significantly higher noise than the other antennas and was dropped from the observations. For a specific description of the original calibration steps see Attridge (1999).

The reader is referred to H&W for a detailed discussion of how to detect small levels of circular polarization with the VLBA. There we describe three techniques for robustly detecting circular polarization with circularly polarized antenna feeds. In our re-analysis of the 5 GHz survey for circular polarization, we applied the *gain transfer* technique which provides a direct measure of the circular polarization in a source. We were unable to apply the other techniques described in H&W due to both a lack of strong circular polarization signals in the sample (most are a few mJy or less) and the lack of sufficiently bright extended structure.

The application of the gain transfer technique is straight forward, requiring that we simply make no assumption about the circular polarization of a source during self-calibration, i.e. we only assume  $(RR+LL)/2 = \tilde{I}_{model}$ . This will leave uncalibrated the *R/L* complex gain ratio at each antenna. For the source model, we used the best model obtained from the original anal-

<sup>1</sup> Physics Department MS057, Brandeis University, Waltham, MA 02454; e-mail: dhoman@brandeis.edu, jfcw@quasar.astro.brandeis.edu

<sup>2</sup> MIT Haystack Observatory, Westford, MA 01886; e-mail:jattridge@haystack.mit.edu

<sup>3</sup> The National Radio Astronomy Observatory is a facility of the National Science Foundation operated under cooperative agreement by Associated Universities, Inc.

<sup>4</sup> The feed leakage term calibrator, OQ 208, was observed for ten scans on each day to assure outstanding parallactic angle coverage.

ysis<sup>5</sup>, and self-calibrated the data in amplitude and phase. After self-calibration, we removed the effects of antenna feed leakage determined by applying the AIPS task PCAL to the unpolarized source OQ208. This step is crucial as uncorrected feed leakage terms may induce non-closing errors in the parallel hand data. After feed leakage correction, we self-calibrated the data again in amplitude and phase using the same model as before. The data were then carefully edited to remove clearly discrepant polarization data from stokes Q, U, and V in an antenna based manner.<sup>6</sup> These “final” data, could then be used to either (1) solve for the  $R/L$  complex gain ratios by self-calibration assuming no circular polarization in that source ( $RR = \tilde{I}_{model}$ ,  $LL = \tilde{I}_{model}$ ), or (2) look for circular polarization on a source by applying a smoothed set of  $R/L$  complex gains from a sub-set of sources.

The key to gain transfer calibration is determining a smoothed set of  $R/L$  complex antenna gains. As suggested in H&W, we initially used nearly the entire 40 source sample to produce a smoothed set of gains. The large sample size was a great asset, and by smoothing the gains over several hours and averaging over many sources, we were insensitive to the particular characteristics (such as strong circular polarization) of any one source. We then applied this smoothed set of gains back to the sources, imaged in circular polarization, and removed the most strongly polarized sources from contributing to the smoothed gains. We repeated this process through a few iterations until there were no sources with apparent CP  $\geq 0.12\%$  that contributed to the smoothed gains.<sup>7</sup> This cutoff gave thirteen sources contributing to the smoothed gains with a boxcar averaging window of six hours. Our main results are insensitive to both the details of which sources contribute to the gains, and our choice of smoothing function and time-scale.

The reader is referred to H&W for a detailed discussion of the uncertainties associated with circular polarization observations with circularly polarized feeds. Here we would like to briefly remind the reader of two points. (1) While it is important to remove feed leakage terms from the parallel hand data, contributions from the small uncertainties in the determination of the feed leakage terms are insignificant relative to the gain uncertainties. (2) Beam squint, resulting from pointing errors, shows up as a pure amplitude gain effect and is therefore naturally included in our estimate of gain uncertainties. In the appendix we have refined our estimate of the gain calibration uncertainties as presented in H&W.

As a final check on our results, we divided the single 48-hour data set into two sub-sets and imaged each separately in CP. This provided a direct test of our understanding of the uncertainties from all but the longest time-scale effects ( $> 12\text{h}$ ). We found no significant differences between the two parts of the 48-hour observation.

### 3. RESULTS

Table 1 lists our results, and Figure 1 presents an image of the circular polarization distribution of a typical source (PKS 0607-157). The sources in this sample tend to be strongly core dominated, and the CP we observe is coincident with the bright VLBI cores. Any small displacements from the VLBI cores do not appear significant within our positional uncertainties which are approximately a beam-width divided by the SNR of the CP

<sup>5</sup> In a few cases, we found that better source models could be made, and in those cases, we used the revised models.

<sup>6</sup> The careful editing in total intensity done during the original analysis was preserved. Edits were always applied to all four cross-correlations.

<sup>7</sup> This includes eliminating 14 weak sources ( $< 800\text{ mJy}$ ) which would not produce at least 1 mJy of CP at 0.12%.

measurement. For this reason, we simply report the measured CP as a fraction of the peak total intensity. The uncertainties and limits listed in Table 1 are dominated by gain calibration uncertainties which are estimated in the appendix. The total quoted uncertainty,  $\sigma$ , includes both the gain uncertainty and the RMS noise in the stokes V map, added in quadrature. The limits in Table 1 are the largest of 1 mJy,  $|V_{peak}| + 1\sigma$ , or  $2\sigma$ .

## 4. DISCUSSION

### 4.1. Detection Rate of Circular Polarization

Figure 2 compares our detection rates for circular polarization for BL Lacs and quasars with the sample of RN&S (also at 5 GHz). For this comparison we have divided by the total VLBI flux (rather than the peak VLBI flux) to better compare to the Australian Telescope Compact Array (ATCA) integrated measurements. Our detection rates are very similar to those of RN&S.

We can do a similar comparison to the 15 GHz VLBI sample of H&W. Here we compare the peak values for fractional circular polarization,  $m_c$ , in our 5 GHz measurements to  $m_c$  of the integrated core at 15 GHz, including model components out to 1.5 mas. This comparison essentially eliminates resolution based differences between the samples. While we find only 2/36 quasars or BL Lacs with  $|m_c| \geq 0.3\%$  in the 5 GHz measurements presented here, the 15 GHz sample of H&W has a significantly higher detection rate for strong CP. There are five closely spaced ( $\sim 2$  month intervals) epochs in H&W which include the same 11 quasars and BL Lacs, three of which show repeated detections of CP. Averaging over the epochs in H&W, we have a mean of 2.4/9.6 detections of  $|m_c| \geq 0.3\%$  from the quasars and BL Lacs strong enough in total intensity in those epochs to have detectable CP at this level. Although the total number of sources in H&W is small, this detection rate is nearly five times that seen here at 5 GHz, and we note that most of the detections in H&W are  $\geq 0.5\%$  CP, and we observe no source with CP that strong in this 5 GHz sample.

The higher incidence of strong circular polarization detections in H&W may be due to one of three possible causes: (1) random fluctuations in small samples, (2) a broad frequency dependent effect, or (3) source selection criteria. We can evaluate option (1) by assuming simple binomial statistics based on our 5 GHz observations (i.e. assume the chance of observing  $|m_c| \geq 0.3\%$  is  $\approx (2 \pm \sqrt{2})/36$ ). We find we would need approximately a 2.5 sigma random variation to explain the 15 GHz results of H&W. Any broad frequency dependent effects, option (2), depend on the generation mechanism of the circular polarization. While both intrinsic CP and Faraday conversion have specific, frequency dependent signatures, the inhomogeneous, self-similar nature of VLBI radio cores complicates the analysis considerably (e.g. Jones (1988)) and may lead to a flat  $m_c$  spectrum for both mechanisms (Wardle & Homan 2001).

With no clear frequency dependent effect, we suspect that source selection criteria, option (3) above, may explain the higher levels of circular polarization observed in H&W. The sample of H&W was part of multi-epoch monitoring program of the strongest, most currently active blazars (Homan et al. (2001); Ojha et al. in prep.), and the three quasars with high levels of CP were undergoing violent core outbursts during the

observations. This is consistent with the report by RN&S of a significant correlation between overall source variability and fractional CP. For RN&S, who have only integrated observations, the correlation with source variability may be confused by a correlation with overall source “compactness”, as extended structure will decrease both the fractional CP of a source and its fractional variability. For the VLBI observations of H&W compactness is not an issue, and the higher levels of fractional CP appear correlated with the selection criteria of currently active sources for that sample.

It is unclear how current core outburst events may lead to increased fractional circular polarization via the intrinsic mechanism. Outbursts are typically associated with shocks that tend to order the magnetic field and increase particle densities. Increased particle densities should not enhance the *fractional* contribution of intrinsic circular polarization, and it is difficult to imagine how the *uni-directional* field necessary for intrinsic CP should be preferentially enhanced by a shock. If the unidirectional field is along the jet axis and the shocks are transverse, just the opposite should happen, and the relative contribution from intrinsic circular polarization should decrease. For Faraday conversion, ordered magnetic fields are necessary for both the generation of linear polarization and its conversion to circular polarization. Shocks in the core may very well increase the contribution of Faraday conversion to the circular polarization produced.

#### 4.1.1. Distribution with Source Type

RN&S found no significant difference between the distribution of circular polarization in the quasars and BL Lacs in their sample, although they did find that BL Lacs and quasars had significantly higher levels of CP than radio galaxies. Their detailed analysis was made possible by the great precision ( $\pm 0.01\%$ ) with which ATCA can measure integrated CP. Due to our higher uncertainty ( $\sim \pm 0.05\%$ ), which induces a dependence on source strength, we cannot do a similar detailed analysis. The BL Lacs in our sample tend to be weaker than the quasars and many have upper limits higher than the typical detection level for quasars.

#### 4.2. Correlation with Linear Polarization

Figure 3 is a plot of fractional core circular polarization,  $|m_c|$ , versus fractional core linear polarization,  $m_l$ . Beyond the fact that linear polarization is almost always stronger than circular polarization, there does not appear to be any correlation between linear and circular polarization of the core. This was also noted by RN&S. One might expect that fractional linear polarization, a measure of field order, should correlate with fractional CP, as disordered magnetic fields will not generate significant *net* CP by either the intrinsic or conversion mechanism. The issue is complicated, however, by the possibility of Faraday depolarization in the cores of these objects. Large rotation measures have been observed in the cores of quasars by Taylor (1998, 2000), and if the Faraday effect is occurring in an external screen, the CP will remain largely unmodified<sup>8</sup>, although the linear polarization may be significantly reduced. The scintillation mechanism described by Macquart & Melrose (2000) for the production of CP has no correlation with linear polarization, but is expected to have rapid changes ( $\sim$  minutes–hours) in sign which are not observed in AGN (see §4.3.2).

<sup>8</sup> Thermal particles are inefficient at Faraday conversion compared to Faraday rotation,  $\tau_{rot}/\tau_{con} \sim 2 \times 10^5 (\lambda B)^{-1}$  (cgs), e.g. Jones & O’Dell (1977)

<sup>9</sup> It is interesting to note that two of our  $2\sigma$  measurements, CTA 102 and 3C 454.3, were also detected  $\sim 20$  years ago with the same sign (Weiler & de Pater 1983).

We find no correlation for fractional CP with either total intensity or redshift in this sample.

### 4.3. Comparison to Other Observations

#### 4.3.1. Recent Observations

We have a single source in common with the observations of RN&S: PKS 0454-234. They found  $+0.26 \pm 0.01\%$  integrated circular polarization in 1997.17 at 5 GHz, compared to our  $2.8\sigma$  result of  $+0.16 \pm 0.06\%$  core circular polarization measured 11 weeks earlier (also at 5 GHz). For the source PKS 0607-157 we detect circular polarization of approximately  $-0.7\%$  in January of 1998 at 8 GHz (Homan et al., in prep.), a signal which is stronger, but of the same sign as we report here at 5 GHz in observations made a full year earlier. This kind of short-term sign consistency in CP observations, as well as the possibility for longer-term consistency, is discussed in §4.3.2.

In 3C 279 we observe strong circular polarization for five epochs in 1996 at 15 GHz (H&W); however, in the 5 GHz sample presented here, we do not detect significant CP for 3C 279 in December of 1996 – a little more than two months after the final 15 GHz CP observations by H&W. In Wardle et al. (1998) we argue that the CP in 3C 279 is associated with the core-west (CW) component which appears to be part of a core outburst event in 3C 279 during 1996. This component would have been strongly self-absorbed at 5 GHz in late 1996, so we should not expect to see any CP from it.

#### 4.3.2. Long-term Sign Consistency

Komesaroff et al. (1984) noted that circularly polarized sources tended to have a *preferred handedness* or sign which they maintained over the course of a few years at 5 GHz. In H&W, we observed the same effect at 15 GHz over five epochs, taken at two month intervals during 1996. Here we present evidence that this sign consistency may persist for decades. Between our sample and those of RN&S and H&W, there are six sources with circular polarization detected both recently and  $\sim 20$  years ago (Komesaroff et al. 1984; Hodge & Aller 1977; Weiler & de Pater 1983): 3C 84, PKS 0537-441, 3C 273, 3C 279, PKS 1921-293, and PKS 1934-638. Of those six sources, five have the same sign of circular polarization today as they preferred two decades ago<sup>9</sup>.

Though the statistics are small, this result is potentially very interesting. It suggests a long-lived property of the jets, stable on the time-scale of multiple outbursts, which sets the preferred sign of circular polarization (Homan & Wardle 1999; Wardle & Homan 2001). A natural possibility for this property is the polarity of a net magnetic flux in the jet, reflecting the magnetic flux at the central engine. This is a fundamental parameter in electro-magnetic models of jet production (e.g. Blandford & Payne (1982); Lovelace & Romanova (1995)). A net flux can generate either intrinsic circular polarization or may drive the Faraday conversion process with a small amount of Faraday rotation, e.g. Wardle et al. (1998). Another possible long-term property is the handedness of a helical field which may produce significant quantities of Faraday conversion, e.g. Hodge (1982).

## 5. CONCLUSIONS

We have presented circular polarization results from a survey of the parsec-scale polarization polarization of 40 AGN at 5 GHz. We found 11 circular polarization detections at the  $3\sigma$  level or higher. This nearly quadruples the number of sources detected in CP at VLBI resolutions. We observed only two sources with high levels of CP,  $|m_c| \geq 0.30\%$ , and we believe that current outbursts in the sources observed by H&W could be related to the higher levels of CP detected there. We found no correlation between fractional linear and circular polarization across our sample. This may be due to Faraday depolarization in the cores of AGN which will leave circular polarization unaffected. In comparing these and other recent results to CP observations made  $\sim 20$  years ago, we found that, in five of six

cases, sources have the same sign of CP today as they did 20 years ago. This suggests the presence of a long term property of the jets, such as the polarity of a net magnetic flux, that is stable on the time-scale of multiple outbursts.

## 6. ACKNOWLEDGMENTS

This work has been supported by NSF Grants AST 95-29228 and AST 98-02708. This research has made use of the NASA/IPAC Extragalactic Database (NED) which is operated by the Jet Propulsion Laboratory, California Institute of Technology, under contract with the National Aeronautics and Space Administration. This research has also made use of NASA's Astrophysics Data System Abstract Service.

## APPENDIX

### UNCERTAINTIES FROM GAIN TRANSFER

The calibration of circular antenna feeds for circular polarization is described in detail in H&W. The *gain transfer* procedure allows calibration of the  $R/L$  complex antenna gain ratio<sup>10</sup> at each antenna by self-calibration assuming zero circular polarization ( $\tilde{R}R = \tilde{I}_{model}$ ,  $\tilde{L}L = \tilde{I}_{model}$ ) on a subset of sources, smoothing the derived antenna gains, and applying the smoothed gains to all sources. Figure 4 shows these gains for a typical antenna in our observations.

In H&W, we showed that there were two main contributions to the complex antenna gain ratios: (1) a long-term offset and (2) a short-term rapid variation. Both contributions were of the order of a percent, and while the long-term offset could be easily corrected, the short-term rapid variation went essentially uncorrected. We noted that the short-term rapid variations seemed uncorrelated between antenna, IF, and scan, and used this to crudely estimate our uncertainties from gain transfer calibration.

In this appendix we provide a more detailed analysis of the uncertainties associated with this calibration technique. For a given antenna, assume we have corrected the complex antenna gain ratio, leaving some residual error  $\delta$  in amplitude and  $\phi$  in phase. Under these circumstances, the residual, uncorrected gain ratio can be written for antenna  $a$  as

$$\left( \frac{G_R}{G_L} \right)_a = (1 + \delta_a) e^{i\phi_a} \quad (A1)$$

where both  $\delta$  and  $\phi$  are on the order of 0.005 with the largest contributions from rapid, uncorrelated variations. In the Stokes  $V$  visibilities, these errors show up, to first order, multiplying the total intensity:

$$\tilde{V}_{ab} = \tilde{V}_{true} + \tilde{I}_{ab} [(\delta_a/2 + \delta_b/2) + i(\phi_a/2 - \phi_b/2)] \quad (A2)$$

Here we consider amplitude errors, as only they show up on the phase center and may be confused for a real circularly polarized signal. For point-like sources, phase errors will not contribute to first order, and for sources with significant extended structure, phase errors will appear in an anti-symmetric fashion about the phase center.

The total uncertainty from gain transfer,  $\sigma_{gains}$ , in the fractional circular polarization includes contributions to  $\delta$  from three sources: (1) uncertainty in the determination of the smoothed antenna gains, (2) uncertainty in the true circular polarization of the calibrator sources, and (3) uncorrected rapid variations in the antenna gain ratios.

**Uncertainty in the smoothed antenna gains** is estimated by examining the scan to scan variations of the thirteen sources used to determine the average gains. We computed the RMS variation in the individual gains from the six hour boxcar average determined on these sources. Before computing the RMS, we took a direct average of the variations across all IFs for each scan. This is to avoid having to make any assumptions about the degree of correlation in the variations between IFs<sup>11</sup>. We found an RMS variation for the calibrators of  $(\delta_{cal})_{RMS} = 0.0029$ . The uncertainty in any given six hour average is given by  $(\delta_{cal})_{RMS}/\sqrt{N_{scans}}$ , where  $N_{scans}$  is the number of scans in that averaging period, and the contribution to the circular polarization of a target source is

$$\sigma_{avg} = \frac{(\delta_{cal})_{RMS}}{\sqrt{N_{scans} N_{ant} N_{avg}}}. \quad (A3)$$

For these observations the number of antennas,  $N_{ant}$ , was nine. The number of independent averages,  $N_{avg}$ , which apply to a given source was taken to be two as each source was observed over a period of five to six hours on each of the two days of the experiment. The average numbers of calibrator scans,  $N_{scans}$ , contributing to the gains applied to each source were computed and are listed in Table 2.

<sup>10</sup> The average gain corrections at each antenna have already been removed by earlier rounds of self-calibration which make no assumption about the presence or absence of CP, i.e. they only assume  $(RR+LL)/2 = \tilde{I}_{model}$ .

<sup>11</sup> This RMS result was roughly  $\sqrt{2}$  higher than simply assuming the four IFs were completely uncorrelated in their variations.

**Uncertainty due to real CP on the calibrators** is easily estimated by finding the RMS apparent CP of the calibrators and dividing by the square root of the number of calibrators contributing to a given gain average:

$$\sigma_{res} = (m_c)_{RMS} / \sqrt{N_{cal}}. \quad (A4)$$

For these observations, the RMS peak circular polarization of the calibrators was  $(m_c)_{RMS} = 0.00065$ . As each source (targets and calibrators alike) was observed over a five to six hour period on each day, and the gain averages are done over a six hour interval, each source overlaps with many calibrator sources. Unfortunately, the contributions of each of these calibrator sources were not equal, and we needed to use a weighted average computed from the experiment schedule and listed in Table 2. These weighted averages were determined in a conservative fashion: the calibrator source with the largest contribution (number of calibrator scans that influenced each target scan) to a given source was treated as a 1.0 contribution, and the other calibrators had their *relative* contribution added to this.

**Uncertainty due to random scan to scan gain variations** can be directly computed for each source:

$$\sigma_{ran} = \frac{(\delta_{source})_{RMS}}{\sqrt{N_{scans}N_{ant}}}. \quad (A5)$$

The RMS variation for each source was computed relative to a twelve-hour average on that source, averaging the variations across IF before computing the RMS so that we made no assumption about the extent of correlated variation between IF<sup>12</sup>.

Table 2 lists our results for each of these contributions on every source as well as the total uncertainty,  $\sigma_{gains} = \sqrt{\sigma_{avg}^2 + \sigma_{res}^2 + \sigma_{ran}^2}$ , contributed by our gain transfer calibration.

#### REFERENCES

Attridge, J. M. 1999 Ph.D. Thesis, Brandeis Univ.  
 Blandford, R. D., & Payne, D. G. 1982 MNRAS, 199, 883  
 Bower, G. C., Falcke, H., & Backer, D. C. 1999 ApJ, 523, L29  
 Bridle, A. H., & Greisen, E. W. 1994 AIPS Memo 87  
 Cotton, W. D. 1993 AJ, 106, 1241  
 Fender, R., Rayner, D., Norris, R., Sault, R. J., & Pooley, G. 2000 ApJ, 530, L29  
 Greisen, E. W. 1988 AIPS Memo 61  
 Hewitt, A., & Burbidge, G. 1993 ApJS, 87, 451  
 Homan, D. C., Ojha, R., Wardle, J. F. C., Roberts, D. H., Aller, M. F., Aller, H. D., & Hughes, P. A. 2001 ApJ, in press, astro-ph/0009301  
 Homan, D. C., & Wardle, J. F. C. 1999 AJ, 118, 1942  
 Hodge, P. E. 1982 ApJ, 263, 595  
 Hodge, P. E., & Aller, H. D. 1977 ApJ, 211, 669  
 Jones, T. W. 1988 ApJ, 332, 678  
 Jones, T. W., & O'Dell, S. L. 1977 ApJ, 214, 522  
 Komesaroff, M. M., Roberts, J. A., Milne, D. K., Rayner, P. T., & Cooke, D. J. 1984 MNRAS, 208, 409  
 Lovelace, R. V. E., & Romanova, M. M. 1995 in ASP Conf. Ser. 100, Energy Transport in Radio Galaxies and Quasars, ed. Hardee, P. E., Bridle, A. H., & Zensus, J. A., 25  
 Macquart, J.-P., Kedziora-Chudczer, L., Rayner, D. P., Jauncey, D. L. 2000 ApJ, 538, 623  
 Macquart, J.-P., & Melrose, D. B. 2000 ApJ, 545, 798  
 Napier, P.J. 1995 in ASP Conf. Ser. 82, Very Long Baseline Interferometry with the VLBA, ed. Zensus, J. A., Diamond, P. J., & Napier, P. J., 57  
 Rayner, D. P., Norris, R. P., & Sault, R. J. 2000 MNRAS, 319, 484  
 Roberts, D. H., Wardle, J. F. C., & Brown, L. F. 1994, ApJ, 427, 718  
 Sault, R. J., & Macquart, J.-P. 1999 ApJ, 526, L85  
 Taylor, G. B. 1998 ApJ, 506, 637  
 Taylor, G. B. 2000 ApJ, 533, 95  
 Wardle, J. F. C., Homan, D. C., Ojha, R., & Roberts, D. H. 1998 Nature, 395, 457  
 Wardle, J. F. C., & Homan, D. C. 2001 in ASP Conf. Ser. (in press), Particles and Fields in Radio Galaxies, ed. Blundell, K. M., & Laing, R. A., astro-ph/0011515  
 Weiler, K. W., & de Pater, I. 1983 ApJS, 52, 293

<sup>12</sup> For sources with large scan to scan variations, we obtained essentially the same result if we simply assumed the four IFs were completely uncorrelated, but for sources with smaller variations, the result was approximately  $\sqrt{2}$  smaller if we assumed the IFs were uncorrelated in their variations.

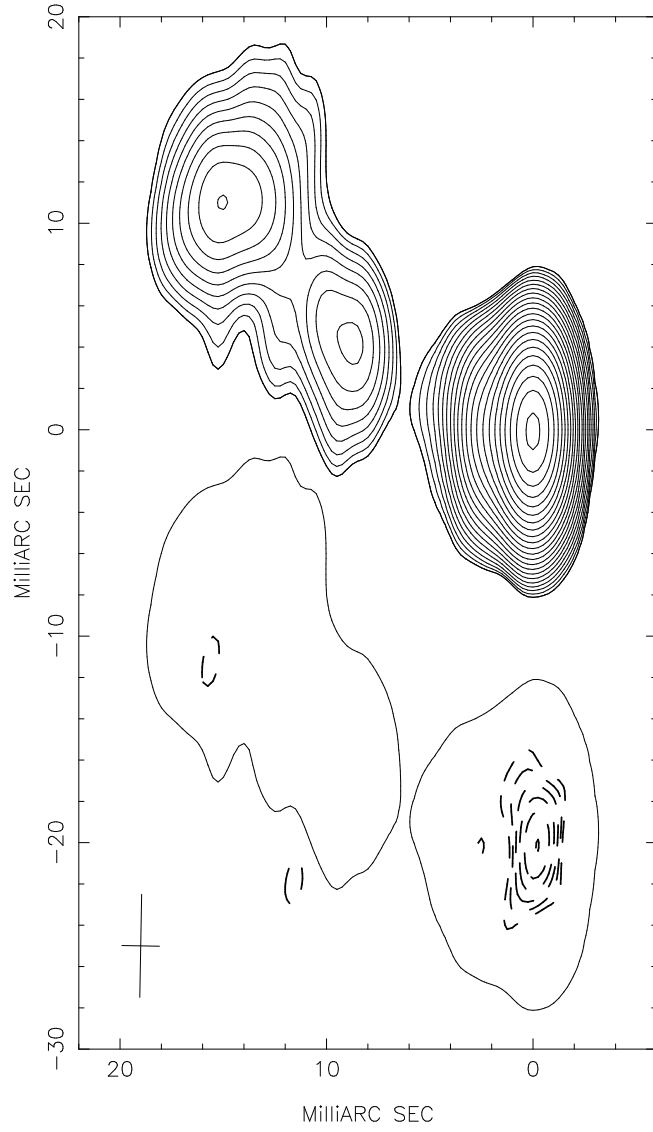
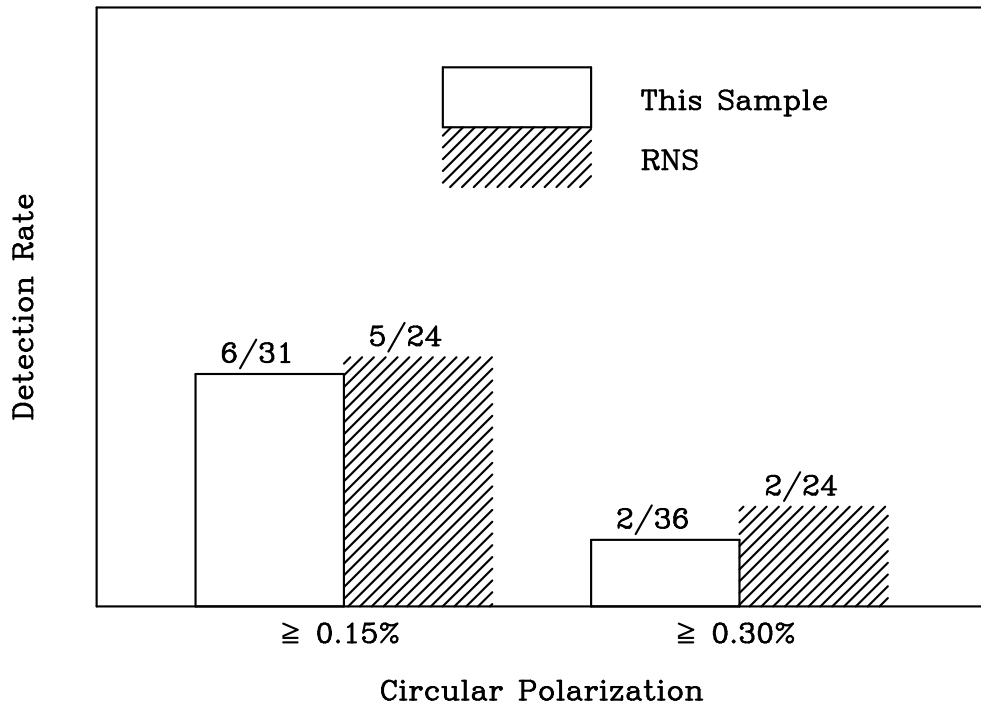


FIG. 1.— Total intensity (lighter contours; factor of  $\sqrt{2}$  beginning at 2 mJy/beam) and circular polarization (darker contours; factor of  $\sqrt{2}$  beginning at  $\pm 0.5$  mJy/beam; dashed contours are negative) of the parsec scale jet of the quasar PKS 0607-157 at 5 GHz, epoch 1996.96. A single Stokes  $I$  contour is overlaid with Stokes  $V$  to show the registration. The peak circularly polarized flux is  $V = -5.7 \pm 1.6$  mJy/beam,  $V/I = -0.18 \pm 0.05\%$ .



### Circular Polarization

FIG. 2.— Detection rates of circular polarization among BL Lacs and quasars. Sources in our sample which are not strong enough to produce a CP signal of at least 1 mJy/beam at a given fractional level are excluded.

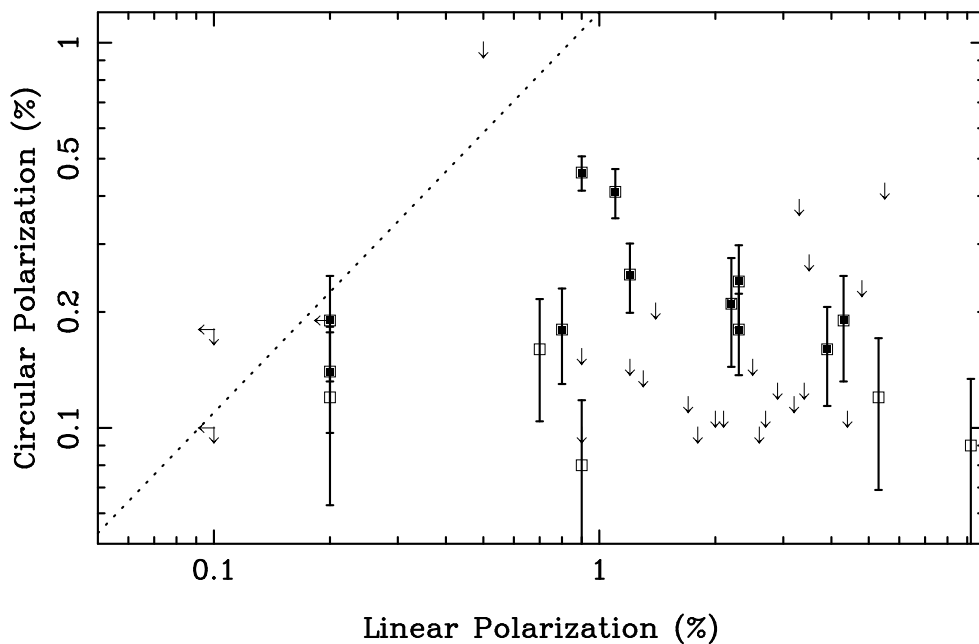


FIG. 3.— Plot of (absolute) fractional core circular polarization versus fractional core linear polarization. The dashed line indicates  $|m_c| = m_l$ . Filled squares indicate  $\geq 3\sigma$  detections. Upper limits are represented by arrows.

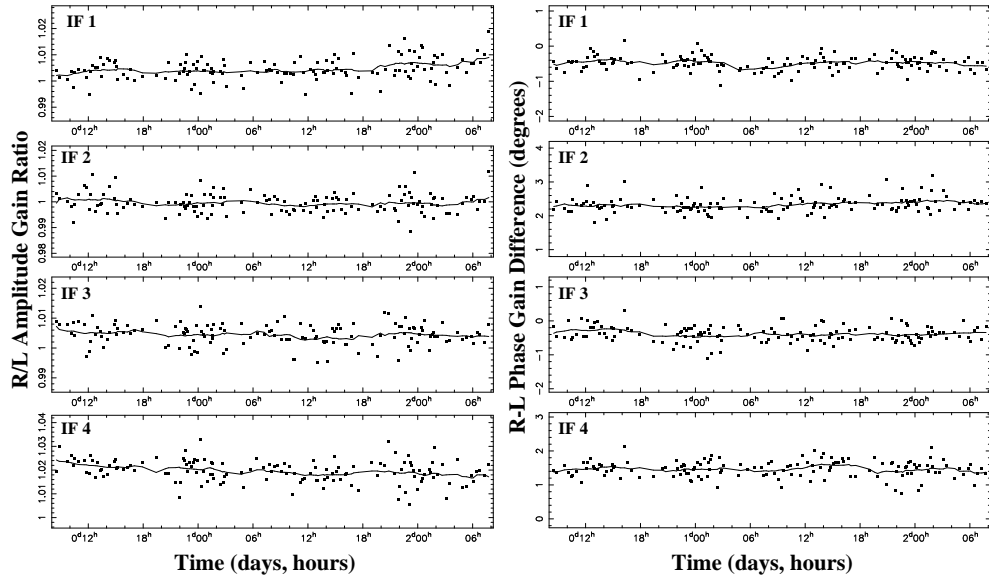


FIG. 4.—R/L amplitude gain ratio corrections (left) and R-L phase gain corrections (right) at the Brewster, WA VLBA station. These are the corrections for the thirteen calibrator sources, assuming zero circular polarization during the final self-calibration (e.g.  $RR = \tilde{I}_{model}$ ,  $LL = \tilde{I}_{model}$ ). A six-hour sliding boxcar average is plotted as a solid line through the points.

TABLE 1  
CIRCULAR POLARIZATION RESULTS.

Object (B1950)	Alt. Name	Redshift	Class	$I_{peak}$ (mJy/beam)	$m_l$ (%)	$V_{peak}$ (mJy/beam)	$m_c$ (%)	$\sigma$
0215+015	PKS	1.715	BL	477	1.4	...	< 0.21	...
0219-164	PKS	0.698	BL	436	2.2	...	< 0.23	...
0219+428	3C 066A	0.444	BL	792	2.9	...	< 0.13	...
<b>0336-019</b>	<b>CTA 26</b>	<b>0.852</b>	<b>Q</b>	<b>1069</b>	<b>4.3</b>	<b>+2.02 ± 0.62</b>	<b>+0.19 ± 0.058</b>	<b>3.3</b>
0403-132	PKS	0.571	Q	639	0.9	...	< 0.16	...
0420-014 <sup>a</sup>	PKS	0.915	Q	2005	2.7	...	< 0.11	...
0422-004	PKS	0.310	BL	357	3.5	-0.71 ± 0.28 <sup>b</sup>	< 0.28	...
0454-234	PKS	1.009	Q	1247	0.7	+1.96 ± 0.70	+0.16 ± 0.056	2.8
0605-085 <sup>a</sup>	PKS	0.870	Q	1832	0.9	...	< 0.10	...
<b>0607-157</b>	<b>PKS</b>	<b>0.324</b>	<b>Q</b>	<b>3161</b>	<b>0.8</b>	<b>-5.72 ± 1.57</b>	<b>-0.18 ± 0.050</b>	<b>3.6</b>
<b>0743-006</b>	<b>PKS</b>	<b>0.994</b>	<b>Q</b>	<b>1489</b>	<b>0.9</b>	<b>-6.82 ± 0.70</b>	<b>-0.46 ± 0.047</b>	<b>9.7</b>
0846+513		1.860	BL	259	3.3	...	< 0.39	...
0851+202 <sup>a</sup>	OJ287	0.306	BL	1053	2.6	...	< 0.10	...
0855+143	3C 212	1.048	Q	102	0.5	...	< 1.0	...
0906+015	DA 263	1.018	Q	234	5.5	...	< 0.43	...
<b>0906+430</b>	<b>3C 216</b>	<b>0.670</b>	<b>Q</b>	<b>485</b>	<b>&lt; 0.2</b>	<b>-0.92 ± 0.28</b>	<b>-0.19 ± 0.058</b>	<b>3.3</b>
1055+018 <sup>a</sup>	PKS	0.888	Q	1565	3.4	+1.25 ± 0.72	< 0.13	...
<b>1150+497</b>	<b>4C 49.22</b>	<b>0.334</b>	<b>Q</b>	<b>817</b>	<b>1.1</b>	<b>-3.39 ± 0.49</b>	<b>-0.41 ± 0.060</b>	<b>6.9</b>
1156+295 <sup>a</sup>	4C 29.45	0.729	Q	1329	2.1	...	< 0.11	...
1253-055 <sup>a</sup>	3C 279	0.536	Q	4711	2.0	-2.95 ± 2.20	< 0.11	...
1334-127	PKS	0.539	Q	3218	5.3	-3.97 ± 1.63	-0.12 ± 0.051	2.4
1404+286 <sup>a</sup>	OQ208	0.077	SyI	1575	< 0.1	...	< 0.10	...
1413+135	OQ122	0.247	BL	743	< 0.1	-0.82 ± 0.45	< 0.18	...
1502+106	OR103	1.839	Q	1240	3.2	...	< 0.12	...
1504-166	PKS	0.876	Q	1475	2.5	+1.36 ± 0.83	< 0.15	...
1510-089	PKS	0.360	Q	1043	4.8	-1.64 ± 0.82 <sup>c</sup>	< 0.24	...
<b>1546+027</b>	<b>PKS</b>	<b>0.413</b>	<b>Q</b>	<b>1958</b>	<b>1.2</b>	<b>-4.88 ± 0.99</b>	<b>-0.25 ± 0.051</b>	<b>4.9</b>
1656+053	PKS	0.879	Q	796	0.2	+0.95 ± 0.45	0.12 ± 0.057	2.1
<b>1842+681</b>		<b>0.472</b>	<b>Q</b>	<b>428</b>	<b>2.2</b>	<b>+0.88 ± 0.28</b>	<b>+0.21 ± 0.066</b>	<b>3.1</b>
<b>1921-293</b>	<b>PKS</b>	<b>0.352</b>	<b>Q</b>	<b>10370</b>	<b>3.9</b>	<b>-16.3 ± 4.8</b>	<b>-0.16 ± 0.046</b>	<b>3.4</b>
1958-179 <sup>a</sup>	PKS	0.650	Q	1736	1.8	...	< 0.10	...
2032+107	PKS	0.601	BL	672	1.2	...	< 0.15	...
<b>2201+171</b>	<b>PKS</b>	<b>1.075</b>	<b>Q</b>	<b>698</b>	<b>2.3</b>	<b>+1.66 ± 0.41</b>	<b>+0.24 ± 0.058</b>	<b>4.0</b>
<b>2223-052</b>	<b>3C 446</b>	<b>1.404</b>	<b>Q</b>	<b>1373</b>	<b>2.3</b>	<b>+2.46 ± 0.59</b>	<b>+0.18 ± 0.043</b>	<b>4.2</b>
2227-088 <sup>a</sup>	PKS	1.561	Q	848	1.7	...	< 0.12	...
2230+114 <sup>a</sup>	CTA 102	1.037	Q	1380	9.2	-1.27 ± 0.61	0.09 ± 0.044	2.1
2234+282 <sup>a</sup>		0.795	Q	820	1.3	-0.71 ± 0.40	< 0.14	...
<b>2243-123</b>	<b>PKS</b>	<b>0.630</b>	<b>Q</b>	<b>1705</b>	<b>~ 0.2</b>	<b>-2.31 ± 0.74</b>	<b>-0.14 ± 0.043</b>	<b>3.1</b>
2251+158 <sup>a</sup>	3C 454.3	0.859	Q	7638	0.9	+6.27 ± 2.91	0.08 ± 0.038	2.2
2345-167 <sup>a</sup>	PKS	0.576	Q	1457	4.4	+0.93 ± 0.64 <sup>b</sup>	< 0.11	...

Note. — Entries with CP detections at  $\geq 3\sigma$  are in bold face. Object classes are from Hewitt & Burbidge (1993), BL = BL Lacerate Object (BL Lac) and Q = Quasar.

<sup>a</sup>Source used to make the smoothed  $R/L$  gain corrections.

<sup>b</sup>Similar strength noise elsewhere in image.

<sup>c</sup>The CP peak is a bit south in the core and the image appears noisy. There also appears to be an approximately anti-symmetric +CP signal of 0.9 mJy/beam north of the core.

TABLE 2  
UNCERTAINTIES FROM GAIN TRANSFER.

Object (B1950)	$N_{\text{scans}}$	$N_{\text{cal}}$	$\sigma_{\text{ran}}$ (%)	$\sigma_{\text{avg}}$ (%)	$\sigma_{\text{res}}$ (%)	$\sigma_{\text{gains}}$ (%)
0215+015	15.5	4.3	0.059	0.018	0.031	0.069
0219-164	16.1	4.5	0.051	0.018	0.031	0.062
0219+428	18.0	5.2	0.034	0.017	0.029	0.047
0336-019	13.8	3.2	0.038	0.019	0.036	0.056
0403-132	13.1	2.9	0.039	0.020	0.038	0.058
0420-014 <sup>a</sup>	12.8	2.8	0.025	0.020	0.039	0.050
0422-004	12.8	2.8	0.054	0.020	0.039	0.069
0454-234	11.7	2.7	0.031	0.021	0.040	0.055
0605-085 <sup>a</sup>	11.9	3.2	0.023	0.020	0.037	0.048
0607-157	11.3	2.8	0.022	0.021	0.039	0.049
0743-006	12.9	4.1	0.027	0.020	0.032	0.046
0846+513	15.1	4.1	0.086	0.018	0.032	0.094
0851+202 <sup>a</sup>	15.4	4.3	0.029	0.018	0.031	0.046
0855+143	16.0	4.8	0.254	0.018	0.030	0.256
0906+015	15.2	4.6	0.058	0.018	0.030	0.068
0906+430	16.2	4.7	0.038	0.018	0.030	0.052
1055+018 <sup>a</sup>	19.3	4.0	0.027	0.016	0.033	0.045
1150+497	18.2	4.2	0.045	0.017	0.032	0.058
1156+295 <sup>a</sup>	18.4	3.6	0.033	0.016	0.034	0.050
1253-055 <sup>a</sup>	18.2	3.0	0.022	0.017	0.037	0.046
1334-127	16.8	2.7	0.025	0.017	0.040	0.050
1404+286 <sup>a</sup>	16.6	3.1	0.024	0.017	0.037	0.047
1413+135	13.3	2.4	0.034	0.019	0.042	0.057
1502+106	13.2	2.5	0.030	0.019	0.041	0.055
1504-166	13.7	2.4	0.030	0.019	0.042	0.055
1510-089	13.1	2.5	0.062	0.020	0.041	0.077
1546+027	12.9	2.6	0.022	0.020	0.040	0.050
1656+053	12.5	3.6	0.036	0.020	0.034	0.053
1842+681	16.6	4.7	0.043	0.017	0.030	0.055
1921-293	15.1	3.4	0.023	0.018	0.035	0.046
1958-179 <sup>a</sup>	18.7	4.1	0.026	0.016	0.032	0.045
2032+107	19.7	4.6	0.032	0.016	0.030	0.047
2201+171	22.6	5.5	0.045	0.015	0.028	0.055
2223-052	23.5	5.7	0.027	0.015	0.027	0.041
2227-088 <sup>a</sup>	23.6	5.5	0.034	0.015	0.028	0.046
2230+114 <sup>a</sup>	22.9	5.4	0.027	0.015	0.028	0.042
2234+282 <sup>a</sup>	23.7	5.4	0.034	0.015	0.028	0.046
2243-123	23.9	5.6	0.028	0.014	0.027	0.042
2251+158 <sup>a</sup>	23.5	5.5	0.021	0.015	0.028	0.038
2345-167 <sup>a</sup>	22.7	5.3	0.027	0.015	0.028	0.042

Note. —  $N_{\text{scans}}$  is the mean number of scans which contribute to the antenna gain averages applied to a source.  $N_{\text{cal}}$  is the weighted number of calibrator sources which determine the antenna gains averages applied to a source, see description in text.

<sup>a</sup>Source used to make the smoothed  $R/L$  gain corrections.